Heliyon 10 (2024) e25910

Contents lists available at ScienceDirect

Heliyon

journal homepage: www.cell.com/heliyon

Research article

Simultaneous two-photon imaging and wireless EEG recording in mice

Bowon Kim [a,b], Weihua Ding [a], Liuyue Yang [a], Qian Chen [c,d], Jianren Mao [a], Guoping Feng [c], Jee Hyun Choi [b], Shiqian Shen [a,*]

[a] Center for Translational Pain Research, Department of Anesthesia, Critical Care and Pain Medicine, Massachusetts General Hospital/Harvard Medical School, Boston, MA, USA
[b] Center for Neuroscience, Korea Institute of Science and Technology, Seoul, Republic of Korea
[c] McGovern Institute for Brain Research and Department of Brain and Cognitive Sciences, Massachusetts Institute of Technology, Cambridge MA, USA
[d] Current address: Zhongshan Institute for Drug Discovery, Shanghai Institute of Materia Medica, Chinese Academy of Sciences, Shanghai, China

ARTICLE INFO

Keywords:
Two-photon
Electroencephalogram (EEG)
Anesthesia
Isoflurane
Global brain state
Multi-dimensional brain activity

ABSTRACT

Background: In vivo two-photon imaging is a reliable method with high spatial resolution that allows observation of individual neuron and dendritic activity longitudinally. Neurons in local brain regions can be influenced by global brain states such as levels of arousal and attention that change over relatively short time scales, such as minutes. As such, the scientific rigor of investigating regional neuronal activities could be enhanced by considering the global brain state.
New method: In order to assess the global brain state during in vivo two-photon imaging, CBRAIN (collective brain research platform aided by illuminating neural activity), a wireless EEG collecting and labeling device, was controlled by the same computer of two-photon microscope. In an experiment to explore neuronal responses to isoflurane anesthesia through two-photon imaging, we investigated whether the response of individual cells correlated with concurrent EEG changes induced by anesthesia.
Results: In two-photon imaging, calcium activities of the excitatory neurons in the primary somatosensory cortex disappeared in about 30s after to the initiation of isoflurane anesthesia. The simultaneously recorded EEG showed various transitional activity for about 7 min from the initiation of anesthesia and continued with burst and suppression alternating pattern thereafter. As such, there was a dissociation between excitatory neuron activity of the primary somatosensory cortex and the global brain activity under anesthesia.
Comparison with existing method(s): Existing methods to combine two-photon and EEG recording used wired EEG recording. In this study, wireless EEG was used in conjunction with two-photon imaging, facilitated by CBRAIN. More importantly, built-in algorithms of the CBRAIN can automatically detect brain state such as sleep. The codes used for EEG classification are easy to use, with no prior experience required.
Conclusion: Simultaneous recording of wireless EEG and two-photon imaging provides a practical way to capture individual neuronal activities with respect to global brain state in an experimental set-up.

* Corresponding author. 149 13th Street, room 6224, Boston, MA 02129, USA.
E-mail address: sshen2@mgh.harvard.edu (S. Shen).

https://doi.org/10.1016/j.heliyon.2024.e25910
Received 31 July 2023; Received in revised form 5 January 2024; Accepted 5 February 2024
Available online 9 February 2024
2405-8440/© 2024 The Authors. Published by Elsevier Ltd. This is an open access article under the CC BY-NC-ND license (http://creativecommons.org/licenses/by-nc-nd/4.0/).

1. Introduction

Brain information flows from one region to others, which is often investigated by the recording of electrical signals among these regions [1]. Locally, the recorded electrical signals reflect ensemble firing. At network levels, the temporal and spatial patterns of these signals reflect circuitry or system level activities [2–4]. There are limitations with these recordings. For example, information processing in the local network could be highly complex which is beyond the firing changes captured by local electrodes. In this case, direct 'visualization' of local network activity in the living brain at cellular and subcellular resolution becomes desirable.

Intravital two-photon imaging provides high spatial resolution, allowing observation of individual cell or dendrite activity [5]. More importantly, the location and morphological features of individual cells can also be recorded longitudinally, providing high-dimensional time-series data to capture cellular activities in vivo. For example, in recent years, fluorescent sensors have been developed to image calcium dynamics, neurotransmitter concentration, endocannabinoid receptor activity etc. at tens of millisecond resolution, revolutionizing neuroscience research [6–9].

As a part of the brain system, both spontaneous and evoked firing of local neurons needs to be seamlessly assimilated to global networks for processing environmental or internal cue. The activity of individual neurons in local brain regions are strongly influenced by global brain state, which can spontaneously change over short periods of time (minutes), such as levels of arousal and attention [10–14]. During the bottom-up processing of sensory information, local neuronal firing may generate global brain activity such as propagating waves and reverberating oscillations [14,15]. On the other hand, local neurons may become disconnected from overall brain activity for various reasons [16,17]. Therefore, to understand the dynamic aspects of the brain system, measuring both local activity and global brain state is desirable.

Electroencephalogram (EEG) is the oldest method for measuring electrical signal of the entire brain, representing the synchronous activity of global and massive neuronal population in the brain with high temporal resolution. Slow rhythms in EEG are well known to indicate overall level of consciousness such as vigilance state and the depth of anesthesia [14,18]. As such, simultaneous recording of EEG during two-photon experiment seems appropriate to analyze the complex local neural network response in the context of global brain state.

Adding EEG equipment to two-photon microscopy and achieving time synchronization between the two set-ups can be cumbersome, particularly with EEG wires. Here, we report combined wireless EEG monitoring using CBRAIN (collective brain research platform aided by illuminating neural activity) [19,20] and intravital two-photon microscopy. Specifically, using wireless EEG transmitter controlled by the same computer of two-photon microscope, we streamlined the experimental set-up for simultaneous EEG recording and two-photon microscopy. We conducted intravital two-photon calcium imaging in both awake and anaesthetized state with concurrent wireless EEG recording, and corroborated data of calcium tracing and EEG.

2. Method

2.1. Animal

Animal experiments protocols were approved by the Massachusetts General Hospital Institutional Animal Care and Use Committee (IACUC). All procedures were conducted following the guidelines established by NIH and the International Association for the Study of Pain. Adult male and female C57/BL6 mice (16–24 weeks old) were purchased from the Jackson Laboratory (ME). Mice were housed with 2 or 3 siblings of the same sex in a temperature and humidity-controlled animal room with 12-h of light/dark cycle (light on at 7 a.m. and light off at 7 p.m.). Food and water were provided ad libitum.

3. Surgery

3.1. Preparation and post-surgery treatment

For electrodes and cranial windows implantation, mice were anaesthetized with isoflurane and placed in a stereotaxic frame (RWD life science, San Diego, USA) with a mouse nose cone connected with anesthetic vaporizer. Vaseline was applied to the eyes to prevent corneas from dehydration. After fur shaving, the skin was disinfected with Povidone-Iodine solution (Aplicare, INC., Neriden, CT, USA) and 70% alcohol swab (BD, Franklin Lakes, USA). After lidocaine (0.2 ml, 1%) infiltration, an incision was made, and part of the scalp was removed. The periosteum and connective tissue over the skull were thoroughly removed with a scalpel, using cotton swab to achieve hemostasis. After surgical procedures, ketorolac tromethamine (Altenex, IL, USA) was injected intraperitoneally at a dose of 5 mg/kg every 12 h for 3 consecutive days. Mice were monitored once daily for postoperative observation.

3.2. Procedures of cranial window and EEG electrodes implantation

Following EEG electrodes implantation, cranial window was created and AAV-CaMKII-GCaMP6f (Addgene, Plasmid #100834, MA, USA) was injected into the primary somatosensory cortex 21–28 days prior to two-photon imaging and EEG recording. After viral injection, cranial glass window was placed. The cranial window, electrode connector and metal bar for head-fixation apparatus were fixed to the skull using dental cement (C&B-Metabond, #171032. Parkell, NY USA). Fig. 1 shows the placement of cranial glass window and EEG electrodes.

EEG screw electrodes were implanted in the contralateral side of the cranial window. Screw placement was performed as described [21]. Specifically, two screw electrodes were implanted in the frontal (AP 1.5 mm, ML 1 mm) and posterior area corresponding to the hippocampus of mouse (AP -2.2 mm, ML 2.2 mm). Two additional screw electrodes (ground and reference screw) were placed at the interparietal bone overlying the cerebellum. Screw electrodes were made of customized wires and 0.8 mm diameter micro screws (custom order, Asia Bolt, South Korea). To minimize interference between the cranial window and electrodes, the exposed portion of screw was less than 2 mm in height. A tungsten wire electrode (PFA-Coated Tungsten Wire, A-M systems, WA, USA) was placed in the neck muscles near occipital bone for EMG signals. Both EEG and EMG electrodes were referenced by the reference electrode in interparietal bone. All electrodes were manually soldered to a female connector (2242-2X08C00DU-P, Oupiin America, INC., CA, USA) which uses1.27 mm PCB socket connecting to CBRAIN.

For the cranial window, a 3 × 3 mm bone flap was removed to observe the somatosensory cortex. Sufficient sterile saline was applied to moisture and hydrate the dura during the procedure. For GCaMP6f expression in the somatosensory cortex, adeno-associated virus 9 (AAV9) carrying GCaMP6f with CaMKII promoter (pENN.AAV.CamkII.GCaMP6f.WPRE.SV40. Addgene. #100834. 1×10^{12} genome copies per ml) was slowly injected at 4–5 sites of the windowed cortex in total volume of 1 μL using a

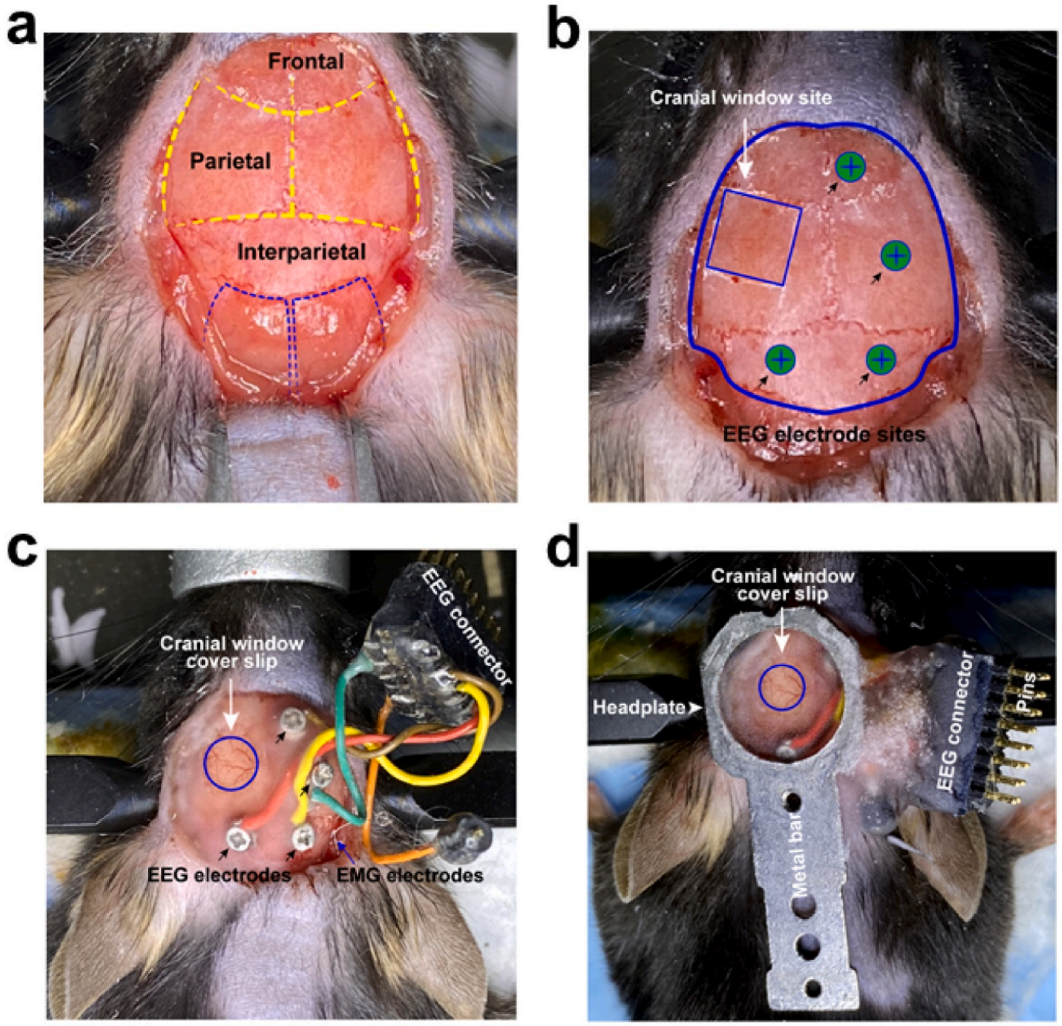

Fig. 1. The Placement of EEG electrode and cranial window on mouse skull during surgery. (a) Landmarks of mouse skull. The mouse skull is divided into frontal, parietal, and interparietal regions by yellow dotted line. The blue dotted line indicates the muscle compartment in contact with the skull and is the site where the EMG electrode is inserted. (b) Locations where electrodes and windows were inserted. Solid blue line marks the boundary of skull and the boundary of craniotomy. Green circles indicate the positions of the frontal, parietal, reference, and ground electrodes in a clockwise fashion. (c) The cranial window and electrode assembly. The picture was taken immediately after cementing the screw electrodes and cranial window to the skull. (d) Sites for the custom-made metal headplate and the electrode. All parts except for the connector and adjacent area around the cranial window were cemented. EEG electrodes were placed with horizontal slant, at a slightly lower level than the horizontal plane, perpendicular to the direction of the lens. (For interpretation of the references to colour in this figure legend, the reader is referred to the Web version of this article.)

Nanoject-III (model #3-000-207, Drummond Scientific Company, PA, USA).

Following virus injection, the cortex was covered by a cranial window layered 5 mm and 3 mm glass coverslips (Warner Instruments, #64–0700 & 64–0720). For cranial window implantation, the 3 mm diameter glass coverslip was inserted into the craniotomy above the pia surface, and the 5 mm coverslip was placed on the skull above the smaller coverslip to cover the craniotomy and adjacent skull. The two coverslips were joined with optical adhesive (#417, Norland Products, INC., NJ, USA).

For head fixation, a custom-made metal headplate was cemented to the coverslips. The connectors and EEG electrodes were secured and fixed using dental cement. To prevent interfering with the lens of the two-photon microscope, the EEG electrodes were slanted and depressed below the metal headplate (Fig. 1d).

3.3. Experimental set-up

Schematic illustration of the experiment set-up was presented in Fig. 2. Mouse was fixed to the customized fixation frame. The head-fixed mouse was kept awake but their movements were confined to a plastic tube. Then the head-fixed mouse was positioned under the two-photon microscope in a vibration-proof chamber. When anesthesia was used, the nose cone anesthesia adaptor was placed to deliver oxygenated anesthetics. To efficiently capture the wireless EEG signals, the Bluetooth wireless receiver was placed within its working distance. The two-photon and CBRAIN recording were controlled by the same computer operating on Windows Operating System. Therefore, we simply align the two-photon data and CBRAIN signal using the time of each file generated at milli second level. We recorded spontaneous calcium signal along with EEG for 10 min as baseline while animals were fully awake with air flowing through the nose cone tube. After baseline recording, we turned on the isoflurane vaporizer to deliver anesthesia (isoflurane 2% V/V in oxygen 2.0 L/min). During anesthesia, the 'end-tidal' gas concentration was monitored using analyzer (AA-8000, BC Biomedical) and mouse body temperature was kept constant by adjusting ambient temperature to parameters determined during habituation sessions.

3.4. In vivo two-photon calcium imaging

Mice were habituated to the experimental environment including the head-fixation device at least 30 min for 5–7 days. Animals placed in the two-photon microscope room for 15 min before imaging experiment. Intravital two-photon calcium imaging was performed using a two-photon laser-scanning microscope (Ultima; Bruker, WI, USA) coupled with a Mai Tai laser (KMC 100; Spectra Physics, CA, USA). The laser was operated at 910 nm and average intensity of laser through the transcranial window was 20–30 mW as previously described [22,23]. The GCaMP6f signal was detected by Hamamatsu multi-alkali Photomultiplier Tubes (Hamamatsu Corporation, NJ, USA) after passing through a 575-nm dichroic mirror and a 525/70 nm band-pass emission filter. The fluorescence images were acquired using Prairie View Software at the frame rate of 6 Hz. The image resolution is 512 × 512 pixels with a 20X, 1.0 NA water-immersion objective (Olympus, Japan).

3.5. EEG recording

We used CBRAIN, a wireless recording and real-time labeling system, for EEG recording. CBRAIN device (2.6 g head stage) wirelessly transmits EEG signals to computer using MATLAB (Mathworks Inc., MA, USA) software. Before monitoring and acquisition of EEG signals, animals were habituated to the CBRAIN device 30 min daily for a week. Locomotion and stress-like behaviors were monitored after the CBRAIN device mounting procedure. On the testing day, signals were recorded at 256 Hz with a 0.1Hz low-pass

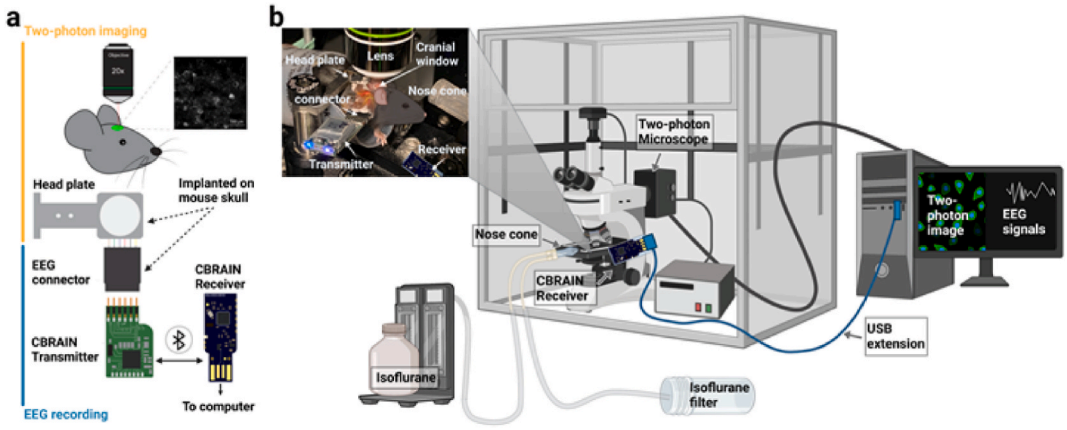

Fig. 2. Schematic illustration of the experiment set-up. (a) A schematic diagram of EEG collection equipment other than skull electrodes. The components in the diagram are the same as in the mouse photo in (b). (b) Illustration of the EEG and two-photon recording environment, composed of a chamber, isoflurane induction instrument, and recording system. (b) created with BioRender.com, photo by Weihua Ding.

filter. Data was saved as 16-int text format with two time stamps marking start and end points of the recording time. CBRAIN can also detect the threshold-based power increase in real time recording after defining the frequency band and threshold before recording. This detection can illuminate the LED light on the top of the CBRAIN device immediately and the signals will be saved in the text file.

3.6. Calcium imaging data processing and analysis

Imaging data was analyzed as previously described [23,24]. Briefly, using the NoRMCorre software package available online and the sequential imaging frames was aligned for motion correction. Individual neurons were selected using a customed script with MATLAB. Calcium fluorescence signals of each neuron were extracted from the aligned imaging data and the signal for each neuron was corrected for background fluorescence changes by subtracting the fluorescence changes from the immediate surrounding. To quantify each neuronal activity, the formula of $\Delta F = (F - F0)/F0$ was used, where F represents the fluorescence signal at a given frame and F0 was calculated from a sliding window of±30 s around the given frame. The baseline correction was carried out by fitting a linear function (MATLAB function robustfit) to the lowpass filtered (cutoff: 0.3 Hz) signal. MATLAB codes for two-photon were adopted from Weihua et al. [23]. and can be found at https://github.com/harnett/Shiqian-analysis.

3.7. EEG data processing and analysis

For EEG data analysis, we used custom-made MATLAB scripts. The CBRAIN data saved as text file can be opened and analyzed using MATLAB. Using the internal counter signal, the raw EEG and EMG data were reconstructed with the period of missed data which majorly caused by transmit errors of Bluetooth. The transmit errors were minimized when the CBRAIN head stage and receiver were close enough (~10 cm, 0 % data loss). For all EEG data analysis, we used custom-made MATLAB scripts and functions in signal processing toolbox. Power spectrogram calculated using spectrogram function (FFT, calculation window size = 1.5 s, 10% moving

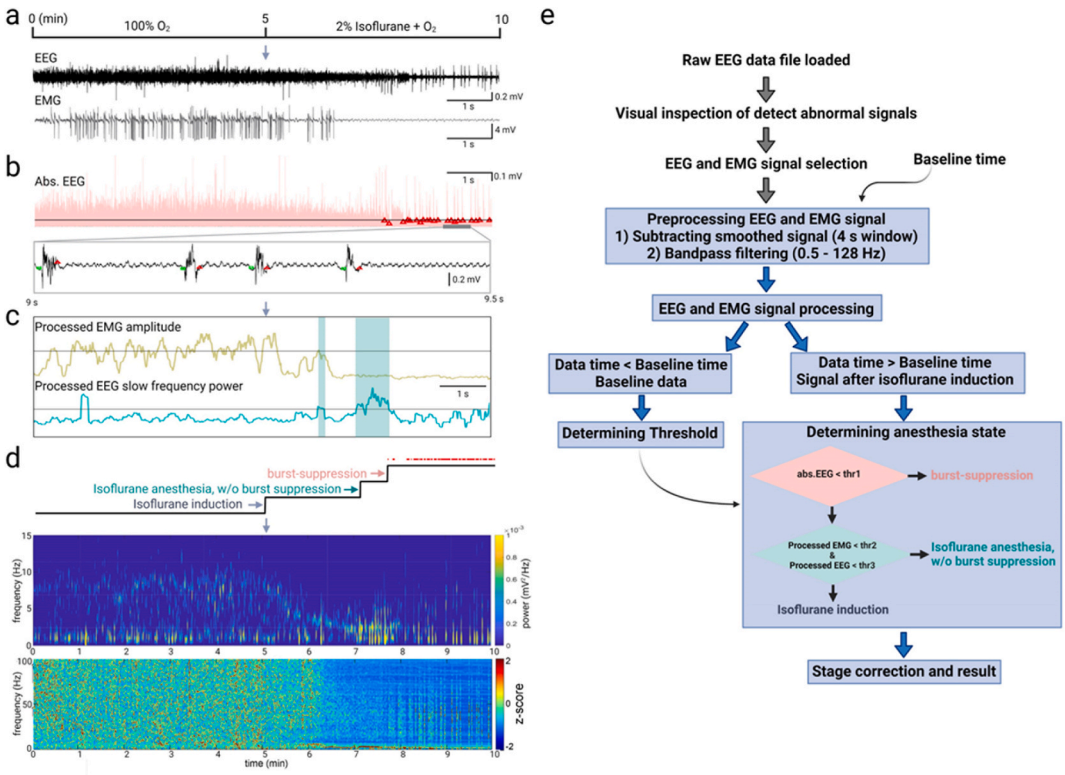

Fig. 3. Description of anesthesia stage classification algorithm using EEG. (a–d) Sample signal traces for classifying isoflurane stages. Shown results were based on baseline recording of 5 min followed by 5 min of recording under isoflurane anesthesia. Grey arrow in each panel indicates the time of turning on isoflurane. (a) Preprocessed EEG and EMG traces for 10 min. (b) Detecting suppression period based on the threshold obtained from the baseline period (0–5 min) with the absolute (abs.) value of the EEG signal as shown in (a). The black line above the pink abs. EEG signal represents the threshold, and the red triangle marks the starting point of the suppression period. The EEG signal during the grey period (9–9.5 s) is shown in lower panel, demonstrating an irregular burst period between the starts (red triangle) and ends (green square) of detected suppression period. (c–d) Results of the categorized stages and EEG spectrograms representing EEG power in each frequency band. Spectrogram and Z-scores plots show different anesthesia stages including bursts suppression. (e) A flow chart of algorithm to classify EEG stages of isoflurane anesthesia. (For interpretation of the references to colour in this figure legend, the reader is referred to the Web version of this article.)

window). In order to clearly show the change in power of the spectrogram, which has smaller values at higher frequencies, we plotted a normalized power spectrogram using z-score ($(x - \mu)/\sigma$). When calculating the z-score, the mean and standard deviation was calculated during baseline period in each frequency bins of the time-frequency spectrogram, and the z-score was calculated for all values in that frequency bin.

Isoflurane anesthesia stage classification algorithm using EEG.

Isoflurane anesthesia was classified into three stages - induction stage, anesthesia stage without burst-suppression, and burst-suppression stage - according to the EEG signals. Analysis code was scripted using MATLAB and is available for download at github.com/ss276/EEG. Fig. 3 shows example traces and flow chart of the data processing. Data analysis comprises four sections: i) EEG and EMG data processing (Fig. 3a); ii) suppression period computation (Fig. 3b); iii) low EMG activity and high slow frequency power computation (Fig. 3c); iv) layout of the categorized stages with spectrograms showing distinct patterns for each stage of anesthesia. (Fig. 3d). During data preprocessing, EEG and EMG signals were detrended from slow fluctuation by subtracting smoothened signal made of the average of every 4 s of raw signal and band-pass filtering (0.5–128 Hz). Suppression events were

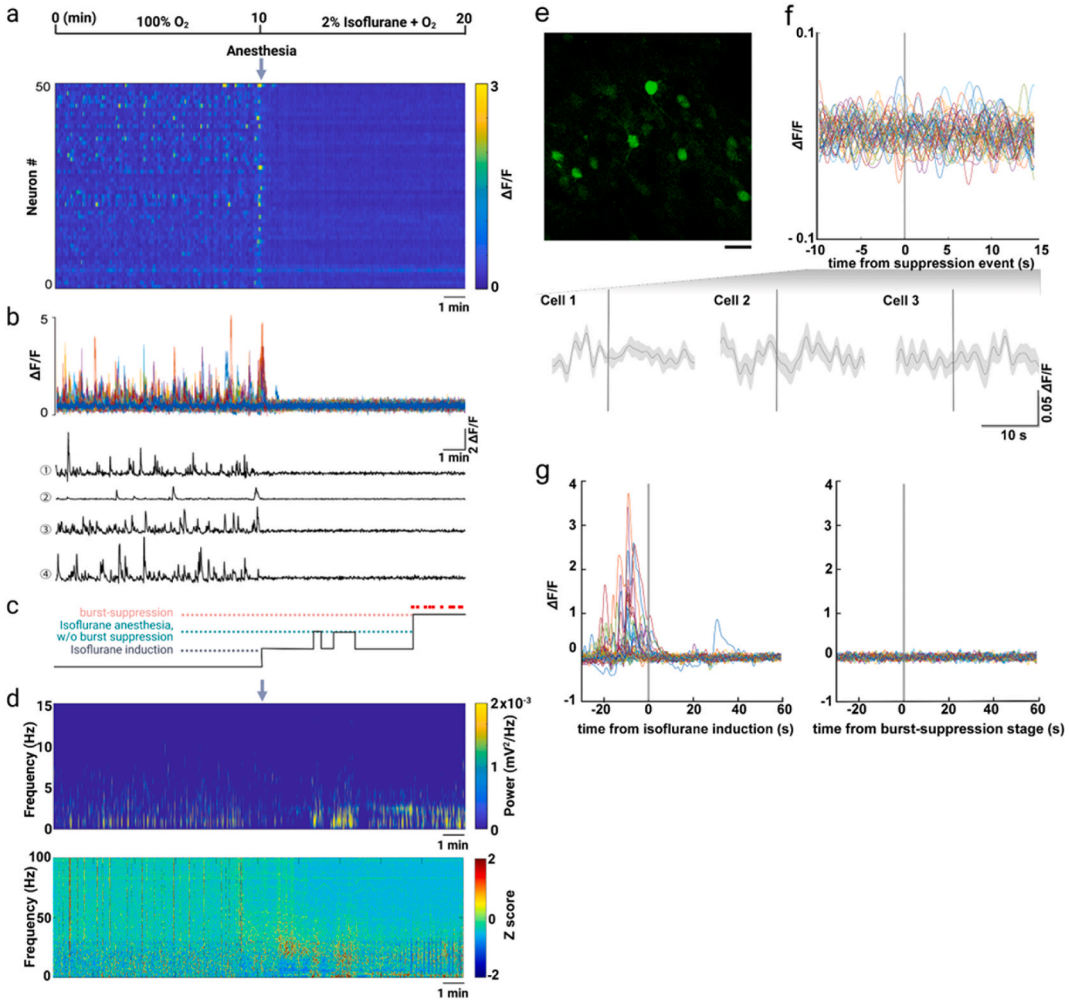

Fig. 4. Simultaneous recording of EEG signal and two-photon imaging. (a) and (b) Calcium dynamics of excitatory neurons in the primary somatosensory cortex (a) Heat map of neuronal calcium dynamics shown for 50 representative neurons. Y axis represents individual neurons, X axis represents time. Color coding represents ΔF/F. (b) Upper panel shows overlay of individual neuron calcium traces for all 50 neurons. Lower panel shows neuronal calcium traces in 4 representative neurons. (c) Categorized stages in simultaneously recorded EEG signals. According to the EEG pattern, stages were divided into the burst-suppression stage (pink), the slow frequency-dominant anesthesia stage without suppression (green), and the induction stage. (d) Spectrogram of temporal changes of EEG power in each frequencies from 0 to 15 Hz (upper panel) and z-scores normalized spectrogram showing relative changes of EEG powers in frequencies between 0 and 100 Hz (lower panel) were aligned with categorized isoflurane stages in (c). The grey arrow in panel (a) and (d) indicates the initiation of isoflurane anesthesia. (e) Representative two-photon image of excitatory neurons in the primary somatosensory cortex (scale bar = 50 μm). (f) The averaged ΔF/F signal of each neurons aligned to detected suppression events. Three individual neuronal ΔF/F tracing were shown, black line-mean, grey shade-standard error of the mean. (g) The time trace of ΔF/F signal in each neuron aligned to the time of isoflurane induction (left panel) and detected burst-suppression period (right panel). Shown figures represent 4 mice. (For interpretation of the references to colour in this figure legend, the reader is referred to the Web version of this article.)

detected by low EMG activity and slow frequency with high power of EEG. The threshold was determined as baseline signals before Isoflurane induction. Burst-suppression stage was computed using absolute values from EEG signal. Brief suppression period was first detected when absolute EEG signal was less than the first threshold (mean + 0.8*std of baseline signal), and then adjusted by applying second, loose threshold (mean + 1.1*std of baseline signal) when gaps between detected periods with first threshold was less than 0.1 s. Anesthesia stage of increased slow EEG activity without burst suppression was determined using absolute values of EMG signal which was less than median value of baseline EMG, and averaged power in delta frequency ranges which was higher than threshold (<2Hz, threshold is the mean + 2 std of baseline). The power spectrogram was calculated using a MATLAB built-in spectrogram function), which applied FFT to every 1.5 s data window with 0.15 s sliding window. If the anesthesia stages became unstable and the time interval between same stages was less than 10 s, the gap was reconstructed as contiguous stage.

4. Results and discussion

Fig. 4 shows representative two-photon and EEG results which were recorded simultaneously. To capture concurrent changes in two-photon imaging and EEG signals, isoflurane anesthesia was used. In this set-up, we were able to investigate the correlation between the calcium activity of excitatory neurons in the primary somatosensory cortex and overall brain activity reflected by EEG under isoflurane anesthesia. In the time trace, the calcium signals of somatosensory excitatory neurons almost disappeared within 30 s after the initiation of isoflurane anesthesia, while the EEG demonstrated gradual changes including increased delta power at around 156-s, and burst-suppression activity at around 448-s after the initiation of isoflurane. Unlike the absence of neuronal activity in the two-photon imaging, the EEG signal showed burst activity which was characterized by a large waveform following 'silent' activities, during burst-suppression period.

Here, we recorded EEG signals and two-photon images simultaneously in awake state and under isoflurane anesthesia, and described the detailed method for acquiring them. In the experiment set-up, EEG signals reflected the overall brain state under isoflurane anesthesia, while two-photon imaging captured individual neuronal activities. This method provides two sets of information: the macroscopic activity of the whole brain and the high-resolution activity of local brain regions. Acquiring additional EEG in two-photon experiment takes approximately 30 min of additional surgery time for electrode insertion as described in the Method section. Compared with existing methods of simultaneous wired EEG and two-photon recording [25–33], the reported method here offers several advantages. CBRAIN head stages [19] can be reused for many years by replacing batteries once every 1–2 years, reducing the cost while enhancing accessibility. Another advantage of using CBRAIN is that it can automatically detect sleep states or slow frequency increases, using existing built-in algorithms of CBRAIN device, with no prior experience with EEG analysis required [19]. In addition, CBRAIN supports off-line analysis, as identifying isoflurane stages shown in this manuscript. Through recording EEG signals and two-photon images together, we found that the excitatory neurons in the primary somatosensory cortex quickly became quiescent and remained 'dormant' in terms of calcium dynamics, regardless of EEG activities. Therefore, it is presumed that the somatosensory cortex was more sensitive to isoflurane, and EEG signals were likely generated by areas other than the somatosensory cortices, including regions that process internal information under anesthesia, such as the ascending reticular activating system. Recording electrical activity of brain is a traditional method with high temporal resolution. Depending on sampling frequency and electrode impedance, signals can reflect the ensemble activity of a large population of neurons or single neuronal spikes. Researchers have found that local electrical features such as increased power, synchrony, cross-frequency-coupling in certain frequency bands represent activation of local neuronal circuits and provide coherent time window for neuronal communication [34–37]. However, electrophysiological recording does not resolve spatial information like optical imaging. Therefore, the method described in this manuscript joins a growing body of literature of simultaneous EEG and two-photon recording, to accommodate experimental needs [30–33].

Our work provides a method to measure local and global brain activity together to understand state-dependent local information processing. Global states of brain such as sleep-wake, vigilance and attentional state are orchestrated by various regulatory pathways [38,39] and could be captured by EEG slow rhythms, representing synchronized activity of many neuronal populations. Researchers showed that EEG synchronization highly correlated with the neuronal responses in two-photon images in a cell-type specific manner [26], with large cell-type variations. Our reported method could facilitate future investigation of individual neuronal dynamics with consideration of the global brain state.

Funding

Shiqian Shen lab received support from NIH R61NS116423, NIH R35GM128692, NIH R01 AG 070141, AG082975-01A1, NIH R03 AG067947, NIH R61 NS126029 and NSF EAGER Award ID2334666. Weihua Ding received support from the Borsook Project. The K. Lisa Yang and Hock E. Tan Center for Molecular Therapeutics in Neuroscience at MIT supported work related to two-photon microscopy in Guoping Feng lab. Bowon Kim received support from Korea Health Technology R&D Project through the Korea Health Industry Development Institute (KHIDI), funded by the Ministry of Health & Welfare, Republic of Korea (grant number: HI21C1234).

Data availability statement

all experiment data are available upon request.

CRediT authorship contribution statement

Bowon Kim: Writing – original draft, Methodology, Investigation, Data curation. **Weihua Ding:** Writing – original draft, Methodology, Investigation, Formal analysis, Data curation. **Liuyue Yang:** Data curation. **Qian Chen:** Formal analysis, Data curation. **Jianren Mao:** Formal analysis. **Guoping Feng:** Supervision, Resources, Formal analysis. **Jee Hyun Choi:** Software, Methodology. **Shiqian Shen:** Writing – review & editing, Supervision, Funding acquisition, Conceptualization.

Declaration of competing interest

All authors declare that they have no conflicts of interest.

Acknowledgements

The authors acknowledge MGH IACUC and the animal facility for kind support; Scot Mackeil from MGH Bioengineer Lab for anesthesia equipment maintenance and validation; Department of Anesthesia, Critical Care and Pain Medicine of MGH for generous support. The authors thank Shelley Turok, David Duarte, Emily O'Connor, and Ariel Mueller at Department of Anesthesia, Critical Care and Pain Medicine of MGH for administrative support.

References

[1] A.K. Engel, P. Fries, W. Singer, Dynamic predictions: oscillations and synchrony in top-down processing, Nat. Rev. Neurosci. 2 (2001) 704–716, https://doi.org/10.1038/35094565.
[2] G. Buzsaki, Theta oscillations in the hippocampus, Neuron 33 (2002) 325–340, https://doi.org/10.1016/s0896-6273(02)00586-x.
[3] G. Buzsaki, A. Draguhn, Neuronal oscillations in cortical networks, Science 304 (2004) 1926–1929, https://doi.org/10.1126/science.1099745.
[4] G. Buzsaki, C.A. Anastassiou, C. Koch, The origin of extracellular fields and currents–EEG, ECoG, LFP and spikes, Nat. Rev. Neurosci. 13 (2012) 407–420, https://doi.org/10.1038/nrn3241.
[5] K. Svoboda, R. Yasuda, Principles of two-photon excitation microscopy and its applications to neuroscience, Neuron 50 (2006) 823–839, https://doi.org/10.1016/j.neuron.2006.05.019.
[6] J. Feng, et al., A genetically encoded fluorescent sensor for rapid and specific in vivo detection of norepinephrine, Neuron 102 (2019), https://doi.org/10.1016/j.neuron.2019.02.037, 745-761 e748.
[7] A. Dong, et al., A fluorescent sensor for spatiotemporally resolved imaging of endocannabinoid dynamics in vivo, Nat. Biotechnol. 40 (2022) 787–798, https://doi.org/10.1038/s41587-021-01074-4.
[8] H. Wang, M. Jing, Y. Li, Lighting up the brain: genetically encoded fluorescent sensors for imaging neurotransmitters and neuromodulators, Curr. Opin. Neurobiol. 50 (2018) 171–178, https://doi.org/10.1016/j.conb.2018.03.010.
[9] C.P. O'Banion, R. Yasuda, Fluorescent sensors for neuronal signaling, Curr. Opin. Neurobiol. 63 (2020) 31–41, https://doi.org/10.1016/j.conb.2020.02.007.
[10] D.V. Buonomano, W. Maass, State-dependent computations: spatiotemporal processing in cortical networks, Nat. Rev. Neurosci. 10 (2009) 113–125, https://doi.org/10.1038/nrn2558.
[11] B. Doiron, A. Litwin-Kumar, R. Rosenbaum, G.K. Ocker, K. Josic, The mechanics of state-dependent neural correlations, Nat. Neurosci. 19 (2016) 383–393, https://doi.org/10.1038/nn.4242.
[12] R.V. Raut, et al., Global waves synchronize the brain's functional systems with fluctuating arousal, Sci. Adv. 7 (2021), https://doi.org/10.1126/sciadv.abf2709.
[13] C.D. Gilbert, M. Sigman, Brain states: top-down influences in sensory processing, Neuron 54 (2007) 677–696, https://doi.org/10.1016/j.neuron.2007.05.019.
[14] K.D. Harris, A. Thiele, Cortical state and attention, Nat. Rev. Neurosci. 12 (2011) 509–523, https://doi.org/10.1038/nrn3084.
[15] F. Han, N. Caporale, Y. Dan, Reverberation of recent visual experience in spontaneous cortical waves, Neuron 60 (2008) 321–327, https://doi.org/10.1016/j.neuron.2008.08.026.
[16] J.M. Krueger, J.T. Nguyen, C.J. Dykstra-Aiello, P. Taishi, Local sleep, Sleep Med. Rev. 43 (2019) 14–21, https://doi.org/10.1016/j.smrv.2018.10.001.
[17] V.V. Vyazovskiy, et al., Local sleep in awake rats, Nature 472 (2011) 443–447, https://doi.org/10.1038/nature10009.
[18] M. Murphy, et al., Propofol anesthesia and sleep: a high-density EEG study, Sleep 34 (2011) 283–291A, https://doi.org/10.1093/sleep/34.3.283.
[19] J. Kim, et al., A bird's-eye view of brain activity in socially interacting mice through mobile edge computing (MEC), Sci. Adv. 6 (2020), https://doi.org/10.1126/sciadv.abb9841.
[20] B. Kim, E. Hwang, R.E. Strecker, J.H. Choi, Y. Kim, Differential modulation of NREM sleep regulation and EEG topography by chronic sleep restriction in mice, Sci. Rep. 10 (2020) 18, https://doi.org/10.1038/s41598-019-54790-y.
[21] B. Kim, et al., Differential modulation of global and local neural oscillations in REM sleep by homeostatic sleep regulation, Proc Natl Acad Sci U S A 114 (2017) E1727–E1736, https://doi.org/10.1073/pnas.1615230114.
[22] L. Yang, et al., Electroacupuncture attenuates surgical pain-induced delirium-like behavior in mice via remodeling gut microbiota and dendritic spine, Front. Immunol. 13 (2022) 955581, https://doi.org/10.3389/fimmu.2022.955581.
[23] W. Ding, et al., Highly synchronized cortical circuit dynamics mediate spontaneous pain in mice, J. Clin. Invest. (2023), https://doi.org/10.1172/JCI166408.
[24] W. Ding, et al., Foramen lacerum impingement of trigeminal nerve root as a rodent model for trigeminal neuralgia, JCI Insight 8 (2023), https://doi.org/10.1172/jci.insight.168046.
[25] J. Cox, L. Pinto, Y. Dan, Calcium imaging of sleep-wake related neuronal activity in the dorsal pons, Nat. Commun. 7 (2016) 10763, https://doi.org/10.1038/ncomms10763.
[26] H.J. Alitto, Y. Dan, Cell-type-specific modulation of neocortical activity by basal forebrain input, Front. Syst. Neurosci. 6 (2012) 79, https://doi.org/10.3389/fnsys.2012.00079.
[27] D.A. Dombeck, A.N. Khabbaz, F. Collman, T.L. Adelman, D.W. Tank, Imaging large-scale neural activity with cellular resolution in awake, mobile mice, Neuron 56 (2007) 43–57, https://doi.org/10.1016/j.neuron.2007.08.003.
[28] N. Niethard, A. Burgalossi, J. Born, Plasticity during sleep is linked to specific regulation of cortical circuit activity, Front Neural Circuits 11 (2017) 65, https://doi.org/10.3389/fncir.2017.00065.
[29] H. Zhou, et al., Cholinergic modulation of hippocampal calcium activity across the sleep-wake cycle, Elife 8 (2019), https://doi.org/10.7554/eLife.39777.
[30] M. Thunemann, et al., Deep 2-photon imaging and artifact-free optogenetics through transparent graphene microelectrode arrays, Nat. Commun. 9 (2018) 2035, https://doi.org/10.1038/s41467-018-04457-5.
[31] X. Wu, et al., A modified miniscope system for simultaneous electrophysiology and calcium imaging in vivo, Front. Integr. Neurosci. 15 (2021) 682019, https://doi.org/10.3389/fnint.2021.682019.
[32] L.F. Cobar, A. Kashef, K. Bose, A. Tashiro, Opto-electrical bimodal recording of neural activity in awake head-restrained mice, Sci. Rep. 12 (2022) 736, https://doi.org/10.1038/s41598-021-04365-7.

[33] C.M. McCullough, et al., GRINtrode: a neural implant for simultaneous two-photon imaging and extracellular electrophysiology in freely moving animals, Neurophotonics 9 (2022) 045009, https://doi.org/10.1117/1.NPh.9.4.045009.
[34] K.J. Friston, A.M. Bastos, D. Pinotsis, V. Litvak, LFP and oscillations-what do they tell us? Curr. Opin. Neurobiol. 31 (2015) 1–6, https://doi.org/10.1016/j.conb.2014.05.004.
[35] B. Pesaran, et al., Investigating large-scale brain dynamics using field potential recordings: analysis and interpretation, Nat. Neurosci. 21 (2018) 903–919, https://doi.org/10.1038/s41593-018-0171-8.
[36] J.H. Siegle, M.A. Wilson, Enhancement of encoding and retrieval functions through theta phase-specific manipulation of hippocampus, Elife 3 (2014) e03061, https://doi.org/10.7554/eLife.03061.
[37] V. Kanta, D. Pare, D.B. Headley, Closed-loop control of gamma oscillations in the amygdala demonstrates their role in spatial memory consolidation, Nat. Commun. 10 (2019) 3970, https://doi.org/10.1038/s41467-019-11938-8.
[38] R.E. Brown, R. Basheer, J.T. McKenna, R.E. Strecker, R.W. McCarley, Control of sleep and wakefulness, Physiol. Rev. 92 (2012) 1087–1187, https://doi.org/10.1152/physrev.00032.2011.
[39] C.B. Saper, P.M. Fuller, Wake-sleep circuitry: an overview, Curr. Opin. Neurobiol. 44 (2017) 186–192, https://doi.org/10.1016/j.conb.2017.03.021.